Sensitive SARS-CoV-2 detection in wastewaters using a carbon nanodot-amplified electrochemiluminescence immunosensor

Tamara Guerrero-Esteban [a], Cristina Gutiérrez-Sánchez [a,**], Ana M. Villa-Manso [a], Mónica Revenga-Parra [a,b,c], Félix Pariente [a,b], Encarnación Lorenzo [a,b,c,*]

[a] Departamento de Química Analítica y Análisis Instrumental, Spain
[b] Institute for Advanced Research in Chemical Sciences (IAdChem), Universidad Autónoma de Madrid, Ciudad Universitaria de Cantoblanco, 28049, Madrid, Spain
[c] IMDEA-Nanociencia, Ciudad Universitaria de Cantoblanco, 28049, Madrid, Spain

ARTICLE INFO

ABSTRACT

Given the great utility that having fast, efficient and cost-effective methods for the detection of SARS-CoV-2 in wastewater can have in controlling the pandemic caused by this virus, the development of new dependable and specific SARS-CoV-2 coronavirus sensing devices to be applied to wastewater is essential to promote public health interventions. Therefore, herein we propose a new method to detect SARS-CoV-2 in wastewater based on a carbon nanodots-amplified electrochemiluminescence immunosensor for the determination of the SARS-CoV-2 Spike S1 protein. For the construction of the immunosensor, *N*-rich carbon nanodots have been synthetized with a double function: to contribute as amplifiers of the electrochemiluminescent signal in presence of [Ru (bpy)$_3$]$^{2+}$ and as antibody supports by providing functional groups capable of covalently interacting with the SARS-CoV-2 Spike S1 antibody. The proposed ECL immunosensor has demonstrated a high specificity in presence of other virus-related proteins and responded linearly to SARS-CoV-2 Spike S1 concentration over a wide range with a limit of detection of 1.2 pg/mL. The immunosensor has an excellent stability and achieved the detection of SARS-CoV-2 Spike S1 in river and urban wastewater, which supplies a feasible and reliable sensing platform for early virus detection and therefore to protect the population. The detection of SARS-CoV-2 Spike S1 in urban wastewater can be used as a tool to measure the circulation of the virus in the population and to detect a possible resurgence of COVID-19.

1. Introduction

Coronavirus disease (COVID-19) that causes the severe acute respiratory syndrome is produced by the SARS-CoV-2 virus and was declared a pandemic on March 13, 2020. This outbreak was declared by The World Health Organization emergency of international interest. It has become the leading cause of death worldwide and is also causing a major socio-economic crisis [1]. Millions of people have been infected due to SARS-CoV-2, also causing the death of many of them [2]. For this reason, the scientific community is making great efforts to deepen the study of this pathogen [3–7] and develop rapid tests to make quick decisions to suddenly stop the transmission of this infectious disease and accurately diagnose the coronavirus.

Currently, there are several biomarkers for the detection of SARS-CoV-2 [8]: Viral genomic RNA [9], membrane proteins, and spike glycoproteins. In fact, based on the detection of different proteins, the diagnosis of COVID-19 is being made quickly through antigen tests. This type of tests acquires great importance due to SARS-CoV-2 has 28 different types of proteins [10], all of them can be detected as antigens and include structural proteins such as spike (S), nucleocapsid (N), matrix (M) and envelope (E). The S and N can be used as biomarkers due to their ability to distinguish different types of coronavirus. The glycoprotein S present on the surface of the virus is responsible for the high contagious, since it is directly involved in the mechanism of entry into the host cell through its ability to bind the host angiotensin-converting enzyme 2 receptors (ACE2), in turn determining the level of infectivity and virulence of the virus. It is abundantly expressed on the surface of human lung cells [11,12]. It is the immune dominant antigen and most intensely recognized by the host's immune system [13]. Hence, it has been the target of several immunosensors based on different

detection techniques [14].

At present, researchers have designed several electrochemical [15, 16] and optical [17,18] immunosensors for SARS-CoV-2. Abdulhadee Yakoh et al. have developed a label-less paper electrochemical platform targeting SARS-CoV-2 for diagnosis [19]. Another electrochemical immunosensor has been developed combining the use of magnetics beads with carbon black as a support for the simultaneous detection of S and also of N proteins [20]. Giwan Seo et al. present a field effect transistor (FET) -based graphene sheet-coated biosensor device using a specific antibody against the SARS-CoV-2 S protein [21]. Colorimetric tests have also been developed such as that proposed by Bartolomeo Della Ventura et al. who have made a colorimetric assay based on AuNPs functionalized with antibodies against the surfaces SARS-CoV-2 proteins [22]. All these methods present advantages and also drawbacks.

Lateral flow assays to develop point of care tests SARS-CoV-2 coronavirus immunosensors currently being employed [23,24]. Therefore, although efforts have never stopped to explore faster and more sensitive methods, there is still a high demand for sensitive, selective, affordable, rapid and user-friendly tests to detect SARS-CoV-2 timely and accurately. Compared to electrochemical [25,26] and optical [17], electrochemiluminescent biosensors offer the advantages of the electrochemical and optical detection. Electrochemiluminescence (ECL) has advantages over other spectroscopic techniques, besides providing accurate control of the time and position of the light-emitting reactions. In addition, because an external light source is not required, light scattering related problems are avoided. In this context, ECL based immunosensors can be a powerful analytical device because they combine the specificity of immunoreaction, the high sensitivity of ECL detection, simple instrumentation, and easy signal quantification and therefore they can be employed in the development of reliable and cost-effective analytical methods for detection of specific proteins indicative of disease. In addition, it has been shown that the performance of ECL biosensors is greatly improved through using nanomaterials resulting in promising breeding strategies in ECL biosensor applications [27], in particular, in terms of sensitivity and stability. However, the application of ECL devices for the detection of SARS-CoV-2 is still in its infancy. As far as we know, the only ECL biosensor previously described [28] is based on the detection of RdRp-COVID gene, but no ECL immunosensor for the detection of SARS-CoV-2 Spike protein, despite the fact that it induces the maximum immune response [19], has been described yet.

On the other hand, most of SARS-CoV-2 biosensors developed, in particular electrochemical immunosensors, have been focused on diagnosis and applied to the detection of SARS-CoV-2 in body fluids, such as nasal and saliva [29]. Few early works applied immunological-based methods to detect viruses in raw wastewater have been described to date [30]. However, there is also evidence that the virus is present in urban wastewater and its detection in these samples is a useful tool already known for the epidemiological surveillance of viruses that is being used in the context of the current coronavirus pandemic, since it is an indicator of the circulation of the virus among the population [31–35]. Hence, wastewater has attracted much attention of environmental researchers, and currently there is no doubt that wastewater-based epidemiology is an efficient alternative of tracking the magnitude and distribution of infection agents in communities.

The ability of urban wastewater surveillance to detect mild or asymptomatic cases is one of its main advantages and can be an early warning tool for prompt identification of the presence of SARS-CoV-2 both now and in the future possible outbreaks or subsequent waves of infection and a potential surveillance tool to complement clinical and home tests. The results would be especially powerful as they can create an early warning system that can inform authorities of a potential outbreak.

Hence, the development of sensitive, cost-effective, and rapid methods for SARS-CoV-2 detection in wastewater are essential for widespread, successful implementation of wastewater-based epidemiology for SARS-CoV-2.

In this work, the development of a reliable, sensitive and disposable ECL immunosensor based on CNDs, which act as antibody support and ECL amplifiers, for rapid determination of S1 in various types of water, including urban wastewater, is described.

2. Experimental

2.1. Chemicals

Malic acid, L-arginine, Tris(2,2-bipyridyl) dichlororuthenium(II) hexahydrate ($[Ru(bpy)_3]^{2+}$), bovine serum albumin (BSA), N-hydroxysuccinimide (NHS), N-(3-dimethylaminopropyl)-N'-ethylcarbodiimide (EDC), 2-(N-morpholino)ethanesulfonic acid (MES) and the other compounds used in the preparation of the different buffer solutions used in this work were obtained from Merck (Darmstadt, Germany). Sodium nitrite and 37% (w/w) hydrochloric acid were obtained from Riedel-de-Haën (Seelze, Germany) and Scharlau (Barcelona, Spain), respectively.

SARS-CoV/SARS-CoV-2 Spike antibody (S1-Ab) (40,150-D003), SARS-CoV-2 (2019-nCoV) Spike S1-His Recombinant Protein (S1) (HPLC-verified) (40,591-V08H), SARS-CoV-2 (2019-nCoV) Spike Detection ELISA Kit (KIT40591), Influenza A H1N1 (A/California/04/2009) Hemagglutinin/HA Protein (ECD, His Tag) (11,055-V08H), MERS-CoV Spike/S1 Protein (S1 Subunit, aa 1–725, His Tag) (40,069-V08B1) and SARS-CoV-2 (2019-nCoV) Nucleocapsid-His Recombinant Protein (40,588-V08B) were purchased from Sino Biological Europe GmbH (Eschborn, Germany). Proteins were reconstituted in sterile water. Mouse anti-human HER2 monoclonal antibody (anti-HER2) and recombinant human HER2 standard were purchased as an ELISA kit (Human ErbB2/HER2 DuoSet ELISA DY1129B) from R&D Systems Europe, Ltd.

All the solutions were prepared using deionized water obtained from a Millipore Milli-Q purification system.

2.2. Instrumentation

Integrated screen-printed carbon electrodes (SPCE) with a silver pseudoreference electrode and a carbon counter electrode were supplied by Metrohm DropSens. These SPCE are necessary to use the electrochemiluminescence equipment (ECL) developed by the same company. The ECL experiments were carried out by an ECL cell with a Si-photodiode integrated and with a potentiostat/galvanostat (± 4 V DC potential range, ± 40 mA maximum measurable current) Metrohm DropSens. To perform the measurement, it is necessary a volume of 50 μL in the ECL cell where the electrodes are confined. For electrochemical measurements a Metrohm-Autolab potentiostat PGSTAT 302 N was used. ECL responses have been normalized against control, that is, in the absence of antigen.

Transmission electron microscopy (TEM) images were recorded with a JEOL JEM 2100 instrument.

Elemental analysis of CNDs was recorded using a PerkinElmer 2400 CHN elemental analyzer.

Dried CNDs powder was used to obtain X-ray diffraction (XRD) spectra using an X-pert PRO Theta/2Theta diffractometer from Panalytical.

Fourier transform infrared (FTIR) spectra were recorded using a Brucker IFS60v spectrometer.

UV–Vis absorption and fluorescence spectra were performed on the PharmaSpec UV-1700 spectrometer (Shimadzu) and on a Cary Eclipse spectrofluorophotometer (Varian), respectively. In both cases, quartz cells with 1.0 cm optical path were used.

Atomic force microscopy (AFM) images were taken with an Agilent 5500 microscope and Olympus cantilevers (RC800PSA, 200_20 mm) operating in tapping mode in air. AFM samples were prepared on high ordered pyrolytic graphite (HOPG) electrodes.

2.3. Procedures

2.3.1. Microwave assisted synthesis of CNDs

CNDs were synthesized with a conventional microwave. First, malic acid (1.5 g) and L-arginine (1.5 g) were weighted and dissolved in 5 mL of water. Once dissolved, the solution was introduced and irradiated in the microwave oven at 800 W for 7 min, obtaining a brown solid. This solid was dissolved in water and the resulting solution was filtered with a 0.25 μm nylon syringe filter to remove large particles. The resulting solution was dialyzed using a dialysis membrane with a range of molecular weight cut-offs of 0.1–0.5 kDa (Spectrum Laboratories) for 90 min. The final solution (160.2 mg/mL) was stored at 4 °C.

2.3.2. CNDs diazonium salt electrografting

The electrografting of CNDs diazonium salt was carried out on carbon electrodes (SPCE and HOPG for ECL and AFM experiments, respectively). Firstly, the diazotization reaction of primary aromatic amine groups present at CNDs surface was carried out by mixing 80.1 mg/mL CNDs with 1.5×10^{-2} M NaNO$_2$ and 0.5 M HCl and for 1 h in an ice bath. Then, the reaction mixture with diazotized CNDs was added onto the electrode surface and the potential was cycled between 0.0 V and −0.9 V for 10 cycles at 0.10 V/s. Finally, the resulting electrografted CNDs modified electrode (CNDs/SPCE) was rinsed with water and stored until use.

2.3.3. Preparation of S1-Ab/CNDs/SPCE immunosensor

The first step for immunosensor development was the preparation of the electrografted CNDs modified electrodes (CNDs/SPCE). Then the carboxyl groups present on the surface of CNDs were activated with 10 μL of a mixture of 50 mg/mL EDC and 50 mg/mL NHS prepared in 0.025 M MES (pH 5.0) buffer solution and let stay for 30 min in a wet chamber. Afterwards, CNDs modified electrode was rinsed with 0.025 M MES (pH 5.0) buffer solution and 5 μL of S1-Ab solution (200 ng/mL in 0.025 M MES (pH 5.0) buffer solution) were dropped on it letting to react for 60 min.

After a washing step with 0.025 M MES (pH 5.0) buffer solution, a blocking step to avoid any unspecific binding was implemented by adding 10 μL of 0.1% BSA solution prepared in 0.1 M phosphate buffer (PB) (pH 7.4) and incubation for 30 min. The resulting modified electrode was called BSA/S1-Ab/CNDs/SPCE.

2.3.4. Detection of S1

5 μL of different concentrations of S1 in a 0.01 M buffer solution (PBS) (pH 7.4) prepared by dissolving Na$_2$HPO$_4$ and KH$_2$PO$_4$ in 137 mM NaCl and 2.7 mM KCl aqueous solution with 5% of Tween® 20, were added and incubated for 30 min onto the immunosensor. Subsequently, the S1/BSA/S1-Ab/CNDs/SPCE was placed into the ECL cell and the measurements were performed in 0.1 M PB (pH 8.0) aqueous solution containing the luminophore [Ru(bpy)$_3$]$^{2+}$ (2.0×10^{-3} M). Potential was cycled between 0.0 V and +1.1 V at 0.030 V/s and the ECL signal obtained was recorded.

2.3.5. Detection of S1 in river and urban wastewater

The immunosensor developed was used for the determination of S1 in river and urban wastewater samples from Community of Madrid, Spain. The samples were stored in a refrigerator immediately after collection. The river water was subjected to a previous gravity filtration treatment with a pleated filter to eliminate suspended particles.

The urban wastewater samples (Waste A and B from a rural area and C, D and E from an urban area) were subjected to a preconcentration treatment based on the protocol described by Randazzo et al. [9]. 200 mL of each of the samples were transferred to centrifuge tubes and pH was adjusted to 6.0 with 0.1 N HCl. Then, one part of 0.9 N AlCl$_3$ solution was added for every 100 parts of sample. The tubes were shaken manually, the pH was readjusted to 6.0 and samples was mixed using an orbital shaker at 150 rpm for 15 min at room temperature. Then,

samples were centrifuged at 1700 g for 20 min, supernatant was discarded, and pellet was resuspended in 1.5 mL of 0.01 M PBS (pH 7.4). The concentrated samples were stored at −20 °C until use.

3. Results and discussion

3.1. Development of a sensitive CNDs based immunosensor for SARS-CoV-2

We have developed a sensitive ECL immunosensor for the detection of S1 based on the use of CNDs as antibody supports and ECL amplifiers. Scheme 1 depicts the different stages followed in the immunosensor development. First, the electrode was modified with the synthesized *N*-rich CNDs. The precursors for CNDs synthesis have been wisely chosen, since is crucial for the development of this immunosensor that the obtained CNDs are rich in aromatic primary amines. These functional groups will allow CNDs to be electrografted on carbon electrodes. In addition, CNDs are used as platform for immobilizing the S1-Ab through crosslinking reactions between carboxylic acids present at their surface and primary amines of S1-Ab after activation with EDC and NHS. To avoid unspecific adsorptions the electrode surface was covered by BSA. Finally, the sensing of the S1 is based on the change in the ECL signal produced by the luminophore [Ru(bpy)$_3$]$^{2+}$ due to the antigen-antibody recognition event that takes place at the electrode surface.

All steps followed for the immunosensor developing were characterized and results are discussed below.

As it is explained in detail in the experimental section, CNDs with the properties mentioned above were synthesized from malic acid and L-arginine as starting materials in a microwave oven. Both are natural products as well as the solvent employed, according to environmentally friendly procedure. The precursors were chosen carefully to obtain primary amine rich CNDs, since we have demonstrated lately that CNDs containing in their surfaces aromatic primary amines can be electrografted on carbon electrodes [36] giving very electrochemically active nanostructured electrodes that improves the performance of ECL systems [37]. After purification, the elemental analysis confirms that synthetized CNDs are mainly composed by C, N and O (% C: 35.90, % H: 6.44, % N: 15.11 and % O (calculated): 42.55).

The morphological characterization confirms that the synthetized CNDs are almost circular structures with diameters around 15 nm, as can be seen in the TEM image of Fig. 1A. They appear as individual features probably due to the presence of nitrogen groups on their surface that avoids aggregates formation. Furthermore, it is not observed that they have a defined structure suggesting that the CNDs have a low level of crystallinity in their structure. In fact, the XRD pattern shows a broad band at 22.4°, indicating that the CNDs present a carbon nucleus with a predominantly amorphous structure (Fig. 1B).

The functional groups present in the synthetized CNDs were elucidated from the FTIR spectra of the precursors used in the synthesis and the CNDs (Fig. 1C). CNDs spectrum clearly shows differences compared with the spectra of L-arginine and malic acid. It presents the characteristic wide band centered at 3500 cm^{-1} related to OH and NH$_2$ groups. The bands observed around 1715 cm^{-1} and 2942 cm^{-1} were assigned to the C═O and C–H stretching vibrations, respectively [38]. Finally, bands attributed to C–N bonds at 1450 cm^{-1} and 1377 cm^{-1}, are also observed [39,40].

We are also interested in the optical properties of the synthetized CNDs. The UV–Visible spectrum shows a shoulder at 330 nm, ascribed to the absorption band of the π-π* transition of C═C conjugated units and the n-π* transition of the C═O from the carbon core (Fig. 1D) [41]. In the inset of Fig. 1D, the CNDs solution shows fluorescence when irradiated with a UV lamp while the CNDs solution under ambient light does not. In fact, an emission band at 405 nm is observed when the excitation wavelength is set at 320 nm (Fig. 1D, inset). Moreover, as the excitation wavelength increases from 320 to 500 nm a decrease in the emission intensity is observed. This characteristic behavior of CNDs, is mainly due
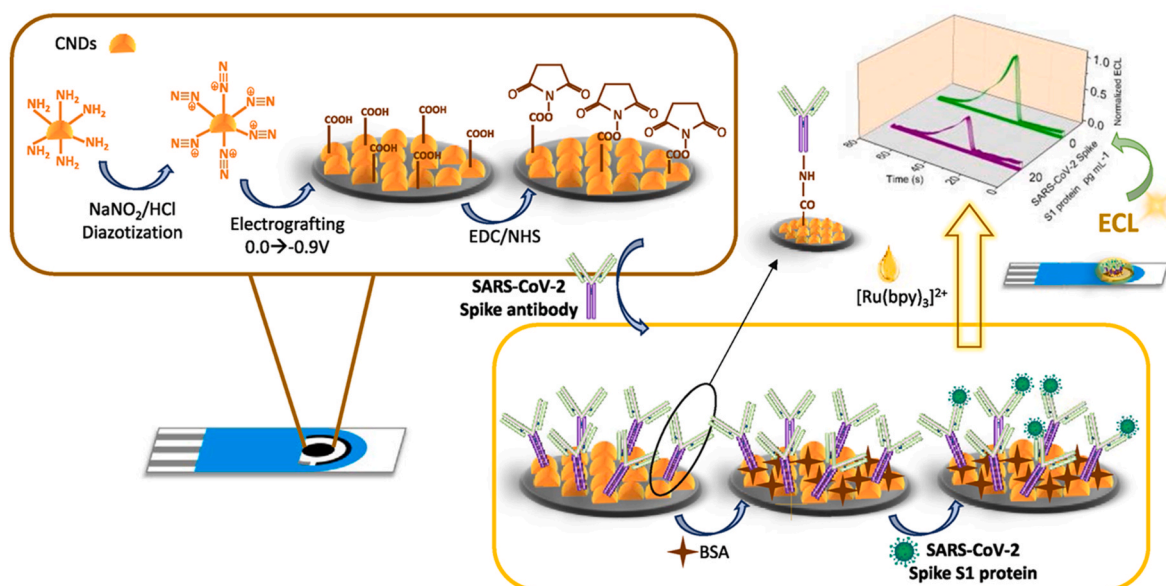
Scheme 1. ECL immunosensor for S1 detection.
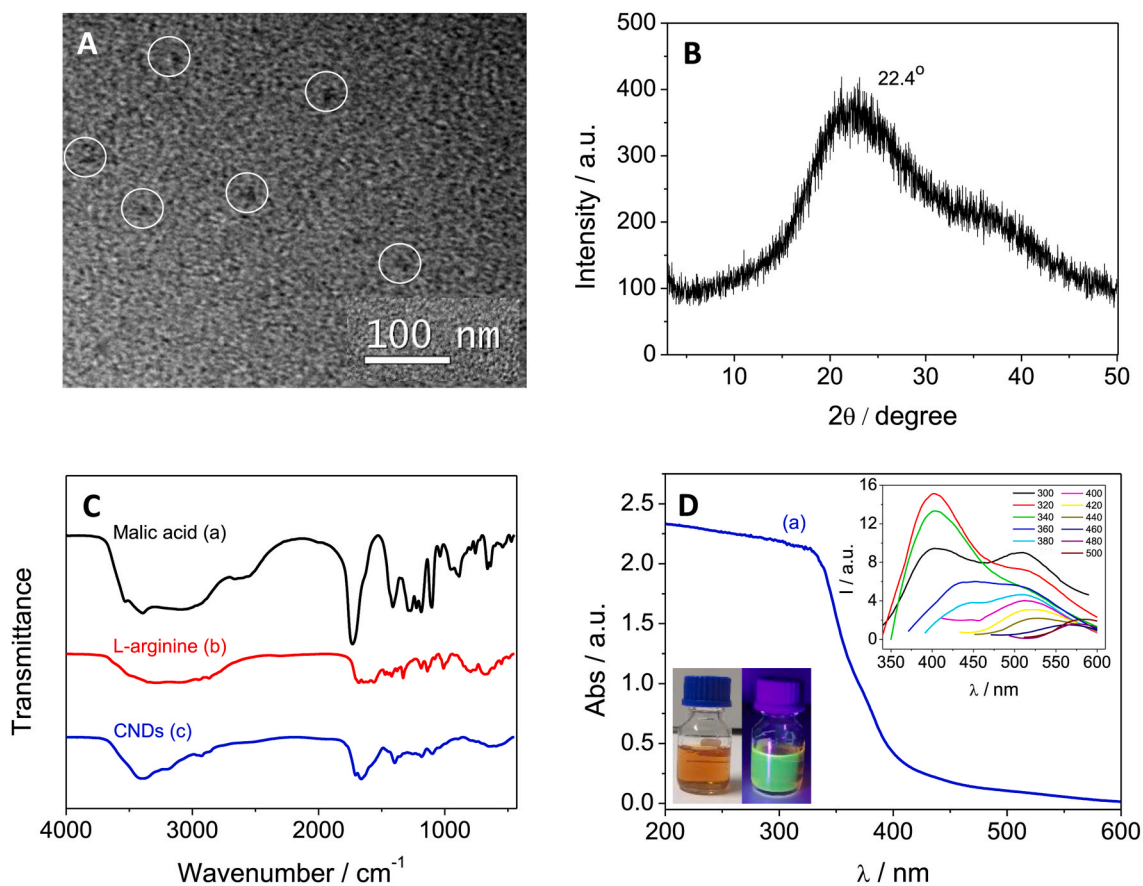

Fig. 1. (A) TEM image of CNDs. B) XRD pattern of CNDs. (C) FTIR spectra of malic acid (a) and L-arginine (b) and CNDs (c). (D) UV–vis (a) and fluorescence emission (inset) spectra of 160.2 mg/mL CNDs aqueous solution. Excitation wavelengths were varied in a range from 300 to 500 nm. Inset: photographs of the CNDs solution under ambient (left) and under UV light at 395 nm (right).

to radiation scattering effects due to the presence of nanoparticles of different sizes [42].

As can be inferred from FTIR studies the prepared CNDs have amine groups on their surfaces, which probably correspond to aromatic amines due to the presence of sp^2 carbons in the core of CNDs. The presence of

these amines allowed the CNDs immobilization on the electrode surface by electrografting (Fig. 2A) of the diazonium salt previously formed by diazotization of the amines with sodium nitrite.

CNDs electrografting on the SPCE surface was carried out cycling the potential between 0.0 V and −0.9 V in 0.5 M HCl. Fig. 2A shows the
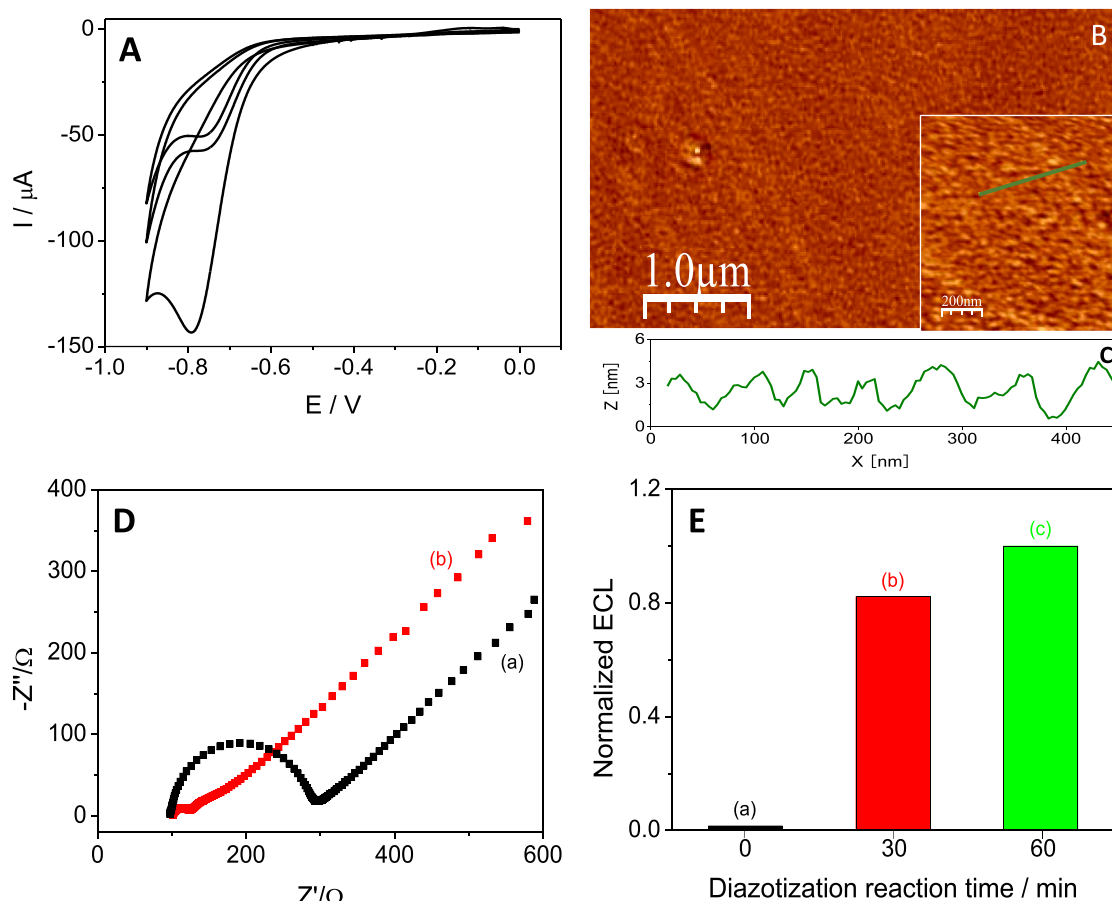
Fig. 2. (A) Cyclic voltammograms performed at SPCE of the electrografting of 80.1 mg/mL CNDs diazonium salt prepared as indicated in experimental section (only the first, fifth and tenth cycles are presented). The measurements were done at 0.10 V/s scan rate. (B) Tapping-mode AFM topographic images of CNDs electrografted on HOPG (CNDs/HOPG). (C) Topographic profile along the line drawn in (B). (D) Nyquist plots recorded in 0.1 M PB (pH 7.0) solution containing 1.0×10^{-2} M $K_3Fe(CN)_6$/1.0×10^{-2} M $K_4Fe(CN)_6$ at a bare SPCE (a) and CNDs/SPCE (b). EIS: frequency range from 10^5 to 5×10^{-2} Hz and potential modulation of 5 mV. (E) ECL responses at bare SPCE (a), CNDs$_{30min}$/SPCE (b) and CNDs$_{60min}$/SPCE (c) in 0.1 M PB (pH 8.0) solution containing 2.0×10^{-3} M $[Ru(bpy)_3]^{2+}$. The ECL measurements were done at 0.030 V/s scan rate.

cyclic voltammograms. It can be seen, that in the first cathodic scan, a reduction process appears with a clearly defined cathodic peak at −0.8 V. In successive scans, the cathodic current decreases. This behavior is characteristic of electrografting processes and is attributed to the reduction of aryldiazonium groups that are efficiently electrografted on the electrode surface [43–46]. In addition, this result corroborates the presence of aromatic amines in the structure of CNDs.

AFM was used to image and to confirm that CNDs were grafted on the electrode surface and to study the morphology of the resulting nanostructured electrode. Fig. 2B shows the HOPG surface after CNDs electrografting, when the reaction time to achieve the CNDs diazonium salt was 60 min. The studies show that the surface is covered with a film composed of a globular disposition of the nanomaterial over the surface and obtaining a complete coating. The coating obtained is homogeneous and it can be observed how the CNDs are electrografted following the direction of the edge planes of the HOPG (see bare HOPG in Fig. S1). A zoom has been made in the sample where it is observed in more detail that the coverage of the surface is total, we could say that there are almost no bare regions because the HOPG surface is not observed. The topographic profile shows particles with a height of about 4–5 nm, compatible with the CNDs height (Fig. 2C) that do not appear at bare HOPG (Fig. S1). We confirm by AFM that the CNDs were electrografted onto the electrode surface.

The resulting CNDs nanostructured electrode (CNDs/SPCE), as one would expect, is more conductive than the bare SPCE. This fact was

confirmed from Electrochemical Impedance Spectroscopy (EIS) analysis. Fig. 2D shows the Nyquist plots obtained for a SPCE and CNDs/SPCE. The impedance analysis has been performed using the classic redox probe, $[Fe(CN)_6]^{3-/4-}$ in 0.1 M PB (pH 7.0) (with 0.1 M KCl). Once the CNDs were electrografted onto the carbon surface, a considerable decrease in the charge transfer resistance (R_{CT}) from 200 Ω to 25 Ω, was observed.

In addition, if CNDs/SPCE is used as electrochemical platform in an ECL system using $[Ru(bpy)_3]^{2+}$ as luminophore, the ECL signal at the CNDs nanostructured electrode is higher than that observed at bare electrode as can be observed in Fig. 3b. Therefore, CNDs improves the conductivity, increases the specific electrode surface area and amplify the ECL signal [47].

Various nanomaterials and co-reactants have been combined as ECL signal amplification agents to improve sensor performance [48,49]. We have previously employed CNDs in ECL systems together with the photoluminescent redox system $[Ru(bpy)_3]^{2+/3+}$ [50–52]. In these approaches the functional groups, such as OH and amino groups, carried by CNDs act as co-reactants in addition to the benefits of nanostructuring the electrode surface.

In order to obtain the highest ECL response, we studied first the effect of the diazotization time. As can be seen (Fig. 2E), the ECL signal increases on increasing the diazotization reaction time from 30 to 60 min. For longer times, practically the ECL response does not change. Therefore, in order to not lengthening the process, 60 min Was chosen as the
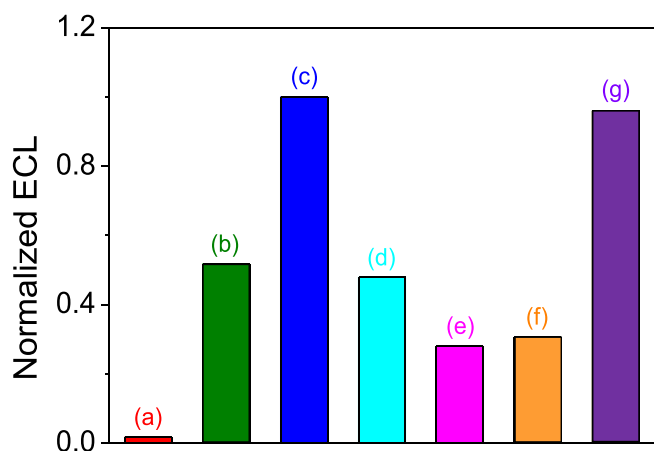
Fig. 3. ECL responses at a bare SPCE (a), CNDs/SPCE (b), BSA/S1-Ab/CNDs/SPCE before (c) and after addition of 20.0 pg/mL S1 (d), BSA/S1-Ab/CNDs/SPCE (prepared without activation with EDC/NHS) (e), BSA/CNDs/SPCE (without antibody) (f) and BSA/anti-HER2/CNDs/SPCE (g) in 0.1 M PB (pH 8.0) solution containing 2.0×10^{-3} M $[Ru(bpy)_3]^{2+}$. The S1 concentration was 20 pg/mL. The ECL measurements were done at 0.030 V/s scan rate. (e), (f) and (g) were recorded after addition of S1 20.0 pg/mL.

optimal CNDs diazotization reaction time for the development of the ECL sensing platform. The number of electrografting cycles and, therefore, the coating of the electrode surface with CNDs was also optimized, 5, 10, 25 and 50 cycles were studied. It was observed that the ECL response increases on increasing the number of cycles from 5 to 10. However, above 25 cycles the ECL signal decreases (data not shown). Therefore, 10 cycles were considered optimal. The stability of the developed CNDs nanostructured electrochemical platform (CNDs $_{60\ min}$/SPCE) has been studied by measuring ECL emission in the presence of $[Ru(bpy)_3]^{2+}$ for 10 days. After this period, the response remains at 97%.

The covalent modification of the electrode with CNDs besides the high stability of the nanomaterial offers additional advantages to those described above, such as the formation of a functional chemical matrix where biomolecules can be covalently bound. Thus, according to Scheme 1, S1-Ab was immobilized on the electrografted CNDs through amide bonds formed between the amino groups present in the protein and the EDC/NHS activated carboxylate groups of CNDs. With this immobilization strategy a stable and accessible immobilization of S1-Ab to the antigen is achieved.

We use the ECL signal to control the successive steps followed in the immunosensor development and as the immunosensor response. The most frequently used ECL-active label is $[Ru(bpy)_3]^{2+}$, because its ECL can be generated in aqueous solutions with a suitable co-reactant and because the emission is intense and fairly stable [37]. Fig. 3 shows the ECL response obtained at each step. The bare SPCE exhibits an almost negligible ECL signal (a) compared to the response after CNDs are electrografted on its surface (b), since, as we described above, CNDs act as amplifying agents of the ECL signal. After S1-Ab immobilization on the electrografted CNDs and BSA addition to prevent nonspecific interactions, there is a considerable increase in the ECL signal (c). We believe that this effect is due to the presence of amino and hydroxyl groups that constitute the antibody that may behave as co-reactants. Capture of 20 pg/mL S1 causes a significant decrease in the ECL signal (d), due to a significant steric hindrance suffered by the ECL probe [Ru(bpy)$_3$]$^{2+}$ after antibody-antigen complex formed. This effect has been previously observed on others ECL immunosensors [53]. This major change in the ECL response allows the detection of S1. Therefore, in order to assess that the ECL signal change observed can be correlated with the S1 recognition event, we carried out different controls. First, the established S1-Ab immobilization protocol was performed without

using EDC/NHS activation. The immunosensor response to 20.0 pg/mL S1 is presented in bar diagram (e) of Fig. 3. It is appreciated a decrease in the ECL signal compared to the response of the immunosensor prepared using activation (see bar d of Fig. 3). This result agrees well with the fact that in the absence of activation, fewer covalent bonds between the antibody and CNDs are formed and those formed are not stable. Thus, there are few antibody molecules on the immunosensor platform to recognize the protein (S1), which results in a decrease in the ECL signal response. A similar ECL signal response is observed (see bar f of Fig. 3) in a second control performed, in which the immunosensor was developed following the protocol established, but without the addition of antibody (S1-Ab). These results confirm the main role that a stable antibody immobilization plays in the final immunosensor response.

Lastly, we also verified that the ECL signal decrease is due to the specific immunological recognition of S1 and the crucial role of the antibody specificity. For this purpose, we used the HER2 antibody (Anti-HER2), which recognizes the protein HER2 but not S1, instead of the S1-Ab. As can be seen in bar (g) of Fig. 3, in this case the ECL response to 20 pg/mL S1 is the same that obtained before recognition of the S1 (see bar c in Fig. 3). No decrease of the ECL signal is observed since there is not any immunological recognition event.

3.2. Optimization of experimental variables

The main experimental variables that may affect the ECL-based immunosensor response, such as pH, $[Ru(bpy)_3]^{2+}$ concentration, scan rate, besides the concentration of S1-Ab, the immobilization time of S1-Ab and incubation time of S1, were evaluated and optimized. The selected criterion was the largest ratio between the ECL immunosensor response in the absence (S_0) or in the presence (S) of 20 pg/mL of S1 (Fig. S2). The highest ECL response was obtained using 0.1 M PB (pH 8.0), 2.0×10^{-3} M $[Ru(bpy)_3]^{2+}$, a scan rate 0.03 V/s with 200 ng/mL of S1-Ab, and immobilization times of 60 and 30 min for the S1-Ab and the S1, respectively. These optimized experimental variables will be used to develop the immunosensor and in the studies described below.

3.3. Analytical performance of SARS-CoV-2 immunosensor

The analytical parameters calculated for the method proposed in this work are shown below. The previously optimized experimental conditions have been considered. Fig. 4A shows that the ECL immunosensor response decreases to increasing amounts of S1. A linear dependence ($r^2 = 0.992$) between ECL signal *vs.* the logarithm of S1 standard concentrations was found up to 240 pg/mL fitting to the adjusted equation ECL (a.u.) = $(-18.1 \pm 0.7) \times 10^{-2}$ log [S1], pg/mL $+ 0.76 \pm 0.01$ (Fig. 4B). The detection (LOD) and quantification (LOQ) limits were estimated according to the criterion $X_{blank} - 3\ S_b/m$ and $X_{blank} - 10\ S_b/m$, respectively, where X_{blank} and S_b are the mean and the normalized standard deviation of the blank signal, respectively, and m is the slope of the calibration plot. The calculated values were 1.2 and 1.9 pg/mL for the LOD and LOQ, respectively.

The reproducibility of the responses obtained with three different immunosensing devices prepared in the same way was also evaluated. The ECL signals obtained for 20 pg/mL S1 standard solution, provided relative standard deviation (RSD) of 5.6%.

In addition, the stability of the immunosensor was studied for 700 s applying consecutive cycles of potential sweep between +0.0 and +1.1 V in 2.0×10^{-3} M $[Ru(bpy)_3]^{2+}$ solution prepared in 0.1 M PB (pH 8.0). The response signal remained very stable and maintained 96% of the initial value (Fig. 4C). The storage stability of the immunosensor was also evaluated. After storage at 4 °C in wet chamber for 44 days, a loss of ECL response with respect to the initial of 8% was observed (Fig. S3).

Also, it has been carried out a study of the selectivity of the immunosensor against several proteins, such as SARS-CoV-2 Nucleocapsid, MERS-CoV Spike S1 and Influenza A virus H1N1. As shown in Fig. 4D, no significant responses are observed for any of proteins assayed, except the
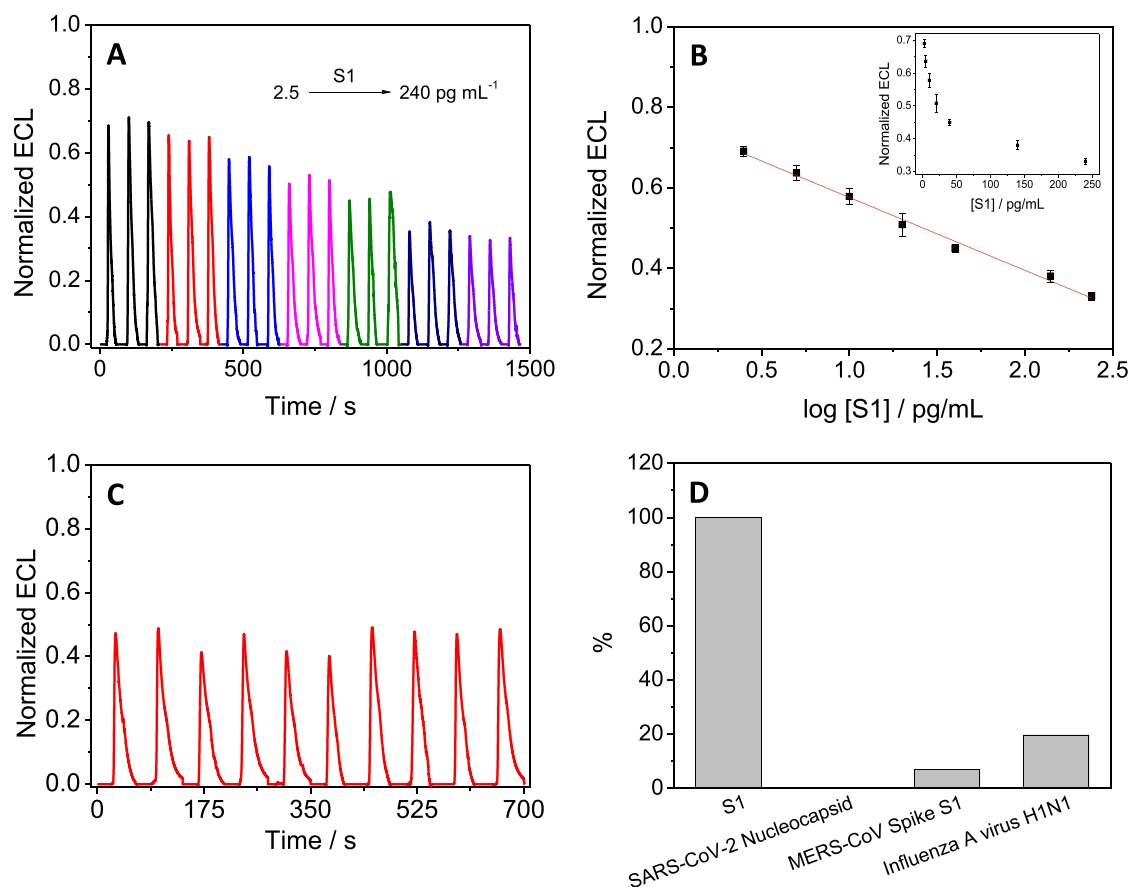
Fig. 4. (A) ECL responses provided by the immunosensor with increasing S1 concentrations, 2.5, 5.0, 10, 20, 40, 140, and 240 pg/mL. (B) Calibration plot obtained with the developed immunosensor for S1 determination. Error bars were estimated from three independent measurements. (C) Analytical signal obtained with the proposed immunosensor under continuous cycles. S1 concentration: 20 pg/mL (D) ECL immunosensor response to mixtures of 20.0 pg/mL of S1 with 20.0 pg/mL of different potential interfering proteins prepared in 0.1 M PB (pH 8.0).

small signal observed in the case of the Influenza A virus H1N1, confirming the immunosensor is quite specific to S1 protein. The response to 20 pg/mL S1 is also included as reference.

The analytical characteristics of the developed ECL-based immunosensor were compared with other S1 immunosensors that have been described so far (Table S1). We have not been able to make a comparison with other ECL-based immunosensors, because as far as we know this is the first ECL immunosensor for S1 prepared to date. From the comparison, we can confirm that our immunosensor has one of the lowest LODs. This good result is due to the combination of the nanomaterial used, CNDs, with the sensitivity of the ECL detection technique employed.

3.4. Determination of S1 in wastewater samples

The real usefulness of the immunosensor developed for the detection of coronavirus SARS-CoV-2 has been evaluated to directly determine S1 in river and urban wastewater samples. Water samples from a river and from rural areas (Waste A and B) were analyzed and compared to results obtained with tap water. The amount of S1 present in all water samples analyzed was no detectable (n.d.) by direct analysis with the ECL method developed, neither with ELISA kit. In Fig. S4, the ECL response without normalizing can be directly appreciated. Thus, the amount of protein in these samples was below the LOD. The recoveries were evaluated by spiking the samples with 40.0 pg/mL S1 obtaining results close to 100% (see Table 1). However, direct determination of S1 in

Table 1
Determination of S1 in river and wastewater samples with the developed ECL-based immunosensor and with the colorimetric ELISA kit as a comparative method (n = 3).

Water Sample	Immunosensor			Water Sample	Immunosensor		ELISA	
	S1 Added	S1 Found	Recovery		S1	RSD	S1	RSD
	(pg/mL)	(pg/mL)	(%)		(pg/mL)	(%)	(pg/mL)	(%)
Tap	0	n. d.	-	Waste C	84 ± 7	8.3	87 ± 7	8
	40	43 ± 1	106					
River	0	n. d.	-	Waste D	83 ± 3	3.6	76 ± 7	9.2
	40	40 ± 2	100					
Waste A	0	n. d.	-	Waste E	8.3 ± 0.4	4.8	7.2 ± 0.3	4.2
	40	42 ± 2	105					
Waste B	0	n. d.	-					
	40	41 ± 2	103					

urban wastewater from different locations (Waste C, D and E) gives values presented in Table 1. The results agree well to those obtained by a conventional ELISA methodology, demonstrating the applicability of the immunosensor.

4. Conclusions

In this work, we have developed a sensitive electrochemiluminescent immunosensor for the direct detection of the Spike S1 protein from SARS-CoV-2 coronavirus through the strategy of using electrochemical disposable platforms nanostructured with *N*-rich carbon nanodots (CNDs). The presence of amino groups allows CNDs electrografting on the electrode surface and also the covalent immobilization of the S1-Ab on their surface providing great stability. Furthermore, CNDs amplify the ECL signal in the presence of $[Ru(bpy)_3]^{2+}$. The ECL-based immunosensor has shown a broad linear response with a low detection limit and a high reproducibility, demonstrating the excellent advantages in sensitivity, cost, and operation stability over other immunosensors. Furthermore, this new sensing platform provides a novel method of tracking SARS-CoV-2 to monitor its prevalence though the detection of S1 in river and wastewaters.

Statement of novelty

This work presents the first electrochemiluminiscent (ECL) immunosensor for SARS-CoV-2 wastewater-based epidemiology. Compared to electrochemical immunosensors, ECL immunosensors combine the specificity of an immunoreaction and the higher sensitivity of ECL. It requires simple and portable instrumentation. Therefore, it is a reliable and cost-effective analytical method that can be used at the point of analysis. The proposed sensor has a limit of detection of 1.2 pg/mL spike protein; a standard deviation of 5.6% and stable response. Hence, it is an interesting alternative to the RT-qPCR considered the standard gold for the determination of SARs-CoV-2 in wastewater due to its high sensibility.

Declaration of competing interest

The authors declare that they have no known competing financial interests or personal relationships that could have appeared to influence the work reported in this paper.

Acknowledgment

Appendix A. Supplementary data

Supplementary data to this article can be found online at https://doi.org/10.1016/j.talanta.2022.123543.

References

[1] A.S. Fauci, H.C. Lane, R.R. Redfield, N. Engl. J. Med. 382 (2020) 1268–1269.
[2] D.D. Rajgor, M.H. Lee, S. Archuleta, N. Bagdasarian, S.C. Quek, Lancet Infect. Dis. 20 (2020) 776–777.
[3] I. Santiago, Chembiochem 21 (2020) 2880–2889.
[4] M. Asif, M. Ajmal, G. Ashraf, N. Muhammad, A. Aziz, T. Iftikhar, J. Wang, H. Liu, Curr. Opin. Electrochem. 23 (2020) 174–184.
[5] H.A. Hussein, R.Y.A. Hassan, M. Chino, F. Febbraio, Sensors 20 (2020) 4289.
[6] A. Merkoçi, C.-z. Li, L.M. Lechuga, A. Ozcan, Biosens. Bioelectron. 178 (2021) 113046.
[7] E. Morales-Narváez, C. Dincer, Biosens. Bioelectron. 163 (2020) 112274.
[8] A. Roda, S. Cavalera, F. Di Nardo, D. Calabria, S. Rosati, P. Simoni, B. Colitti, C. Baggiani, M. Roda, L. Anfossi, Biosens. Bioelectron. 172 (2021) 112765.
[9] W. Randazzo, P. Truchado, E. Cuevas-Ferrando, P. Simón, A. Allende, G. Sánchez, Water Res. 181 (2020) 115942.
[10] A. Wu, Y. Peng, B. Huang, X. Ding, X. Wang, P. Niu, J. Meng, Z. Zhu, Z. Zhang, J. Wang, J. Sheng, L. Quan, Z. Xia, W. Tan, G. Cheng, T. Jiang, Cell Host Microbe 27 (2020) 325–328.
[11] L. Mousavizadeh, S. Ghasemi, J. Microbiol. Immunol. Infect. 54 (2) (2021) 159–163.
[12] D. Wrapp, N. Wang, K.S. Corbett, J.A. Goldsmith, C.-L. Hsieh, O. Abiona, B.S. Graham, J.S. McLellan, Science 367 (2020) 1260.
[13] W. Ji, W. Wang, X. Zhao, J. Zai, X. Li, J. Med. Virol. 92 (2020) 433–440.
[14] A. Ahmadivand, B. Gerislioglu, Z. Ramezani, A. Kaushik, P. Manickam, S.A. Ghoreishi, Biosens. Bioelectron. 177 (2021) 112971.
[15] M. Mehmandoust, Z.P. Gumus, M. Soylak, N. Erk, Talanta 240 (2022) 123211.
[16] S. Eissa, H.A. Alhadrami, M. Al-Mozaini, A.M. Hassan, M. Zourob, Microchim. Acta 188 (2021) 199.
[17] T. Stanborough, F.M. Given, B. Koch, C.R. Sheen, A.B. Stowers-Hull, M.R. Waterland, D.L. Crittenden, ACS Omega 6 (2021) 6404–6413.
[18] M. Divagar, R. Gayathri, R. Rasool, J.K. Shamlee, H. Bhatia, J. Satija, V.V.R. Sai, IEEE Sensor. J. 21 (2021) 22758–22766.
[19] A. Yakoh, U. Pimpitak, S. Rengpipat, N. Hirankarn, O. Chailapakul, S. Chaiyo, Biosens. Bioelectron. 176 (2021) 112912.
[20] L. Fabiani, M. Saroglia, G. Galatà, R. De Santis, S. Fillo, V. Luca, G. Faggioni, N. D'Amore, E. Regalbuto, P. Salvatori, G. Terova, D. Moscone, F. Lista, F. Arduini, Biosens. Bioelectron. 171 (2021) 112686.
[21] G. Seo, G. Lee, M.J. Kim, S.-H. Baek, M. Choi, K.B. Ku, C.-S. Lee, S. Jun, D. Park, H.G. Kim, S.-J. Kim, J.-O. Lee, B.T. Kim, E.C. Park, S.I. Kim, ACS Nano 14 (2020) 5135–5142.
[22] B.D. Ventura, M. Cennamo, A. Minopoli, R. Campanile, S.B. Censi, D. Terracciano, G. Portella, R. Velotta, ACS Sens. 5 (2020) 3043–3048.
[23] B.D. Grant, C.E. Anderson, J.R. Williford, L.F. Alonzo, V.A. Glukhova, D.S. Boyle, B.H. Weigl, K.P. Nichols, Anal. Chem. 92 (2020) 11305–11309.
[24] N. Jiang, N.D. Tansukawat, L. Gonzalez-Macia, H.C. Ates, C. Dincer, F. Güder, S. Tasoglu, A.K. Yetisen, ACS Sens. 6 (2021) 2108–2124.
[25] J.C. Soares, A.C. Soares, M.K.S.C. Angelim, J.L. Proença-Modena, P.M. Moraes-Vieira, L.H.C. Mattoso, O.N. Oliveira Jr., Talanta 239 (2022) 123076.
[26] C. Jiang, X. Mu, B. Du, Z. Tong, Micro & Nano Lett. 17 (2022) 49–58.
[27] A. Fiorani, J.P. Merino, A. Zanut, A. Criado, G. Valenti, M. Prato, F. Paolucci, Curr. Opin. Electrochem. 16 (2019) 66–74.
[28] Z. Fan, B. Yao, Y. Ding, J. Zhao, M. Xie, K. Zhang, Biosens. Bioelectron. 178 (2021) 113015.
[29] L. Fabiani, V. Caratelli, L. Fiore, V. Scognamiglio, A. Antonacci, S. Fillo, R. De Santis, A. Monte, M. Bortone, D. Moscone, F. Lista, F. Arduini, Biosensors 11 (2021) 310.
[30] D. Lu, D.Z. Zhu, H. Gan, Z. Yao, Q. Fu, X. Zhang, Sci. Total Environ. 777 (2021) 146239.
[31] N. Neault, A.T. Baig, T.E. Graber, P.M. D'Aoust, E. Mercier, I. Alexandrov, D. Crosby, S. Baird, J. Mayne, T. Pounds, M. MacKenzie, D. Figeys, A. MacKenzie, R. Delatolla, medRxiv (2020), https://doi.org/10.1101/2020.09.01.20185280. https://www.medRxiv.org.
[32] L.C. de Oliveira, A.F. Torres-Franco, B.C. Lopes, B.S.Á.d.S. Santos, E.A. Costa, M.S. Costa, M.T.P. Reis, M.C. Melo, R.B. Polizzi, M.M. Teixeira, C.R. Mota, Water Res. 195 (2021) 117002.
[33] Z.W. LaTurner, D.M. Zong, P. Kalvapalle, K.R. Gamas, A. Terwilliger, T. Crosby, P. Ali, V. Avadhanula, H.H. Santos, K. Weesner, L. Hopkins, P.A. Piedra, A.W. Maresso, L.B. Stadler, Water Res. 197 (2021) 117043.
[34] L. Lundy, D. Fatta-Kassinos, J. Slobodnik, P. Karaolia, L. Cirka, N. Kreuzinger, S. Castiglioni, L. Bijlsma, V. Dulio, G. Deviller, F.Y. Lai, N. Alygizakis, M. Barneo, J.A. Baz-Lomba, F. Béen, M. Cíchová, K. Conde-Pérez, A. Covaci, E. Donner, A. Ficek, F. Hassard, A. Hedström, H. Hernandez, V. Janská, K. Jellison, J. Hofman, K. Hill, P.-Y. Hong, B. Kasprzyk-Hordern, S. Kolarević, J. Krahulec, D. Lambropoulou, R. de Llanos, T. Mackuľak, L. Martinez-García, F. Martínez, G. Medema, A. Micsinai, M. Myrmel, M. Nasser, H. Niederstätter, L. Nozal, H. Oberacher, V. Očenášková, L. Ogorzaly, D. Papadopoulos, B. Peinado, T. Pitkänen, M. Poza, S. Rumbo-Feal, M.B. Sánchez, A.J. Székely, A. Soltysova, N.S. Thomaidis, J. Vallejo, A. van Nuijs, V. Ware, M. Viklander, Water Res. 199 (2021) 117167.
[35] G. La Rosa, L. Bonadonna, L. Lucentini, S. Kenmoe, E. Suffredini, Water Res. 179 (2020) 115899.
[36] C. Gutierrez-Sanchez, M. Mediavilla, T. Guerrero-Esteban, M. Revenga-Parra, F. Pariente, E. Lorenzo, Carbon 159 (2020) 303–310.
[37] W. Miao, Chem. Rev. 108 (2008) 2506–2553.
[38] V.N. Mehta, S. Jha, S.K. Kailasa, Mater. Sci. Eng. C 38 (2014) 20–27.
[39] D.D. Ferreyra, D. Rodríguez Sartori, S.D. Ezquerra Riega, H.B. Rodríguez, M.C. Gonzalez, Carbon 167 (2020) 230–243.
[40] F. Arcudi, L. Đorđević, M. Prato, Angew. Chem. Int. Ed. 55 (2016) 2107–2112.
[41] S. Carrara, F. Arcudi, M. Prato, L. De Cola, Angew. Chem. Int. Ed. 56 (2017) 4891-4891.
[42] S. Zhu, Q. Meng, L. Wang, J. Zhang, Y. Song, H. Jin, K. Zhang, H. Sun, H. Wang, B. Yang, Angew. Chem. Int. Ed. 52 (2013) 3953–3957.
[43] C. Gutierrez-Sanchez, S. Shleev, A.L. De Lacey, M. Pita, Chem. Pap. 69 (2015) 237–240.
[44] M. Delamar, R. Hitmi, J. Pinson, J.M. Saveant, J. Am. Chem. Soc. 114 (1992) 5883–5884.
[45] M. Revenga-Parra, A.M. Villa-Manso, M. Briones, E. Mateo-Martí, E. Martínez-Periñán, E. Lorenzo, F. Pariente, Electrochim. Acta 357 (2020) 136876.

[46] M. Revenga-Parra, C. Gómez-Anquela, T. García-Mendiola, E. Gonzalez, F. Pariente, E. Lorenzo, Anal. Chim. Acta 747 (2012) 84–91.

[47] Y.-M. Long, L. Bao, Y. Peng, Z.-L. Zhang, D.-W. Pang, Carbon 129 (2018) 168–174.

[48] S. Li, J. Luo, X. Yang, Y. Wan, C. Liu, Sensor. Actuator. B Chem. 197 (2014) 43–49.

[49] C. Zhao, L. Niu, X. Wang, W. Sun, Bioelectrochemistry 135 (2020) 107585.

[50] C. Gutiérrez-Sánchez, M. Mediavilla, T. Guerrero-Esteban, M. Revenga-Parra, F. Pariente, E. Lorenzo, Carbon 159 (2020) 303–310.

[51] T. Guerrero-Esteban, C. Gutiérrez-Sánchez, E. Martínez-Periñán, M. Revenga-Parra, F. Pariente, E. Lorenzo, Sensor. Actuator. B Chem. 330 (2021) 129389.

[52] T. Guerrero-Esteban, C. Gutiérrez-Sánchez, T. García-Mendiola, M. Revenga-Parra, F. Pariente, E. Lorenzo, Sensor. Actuator. B Chem. 343 (2021) 130096.

[53] T. Kalyani, A. Sangili, A. Nanda, S. Prakash, A. Kaushik, S. Kumar Jana, Bioelectrochemistry 139 (2021) 107740.